



HAL
open science

Adsorption of proteins on TiO₂ particles influences their aggregation and cell penetration

Romain Vian, Hamideh Salehi, Marion Lapierre, Frédéric Cuisinier, Vincent Cavallès, Sebastien Balme

► To cite this version:

Romain Vian, Hamideh Salehi, Marion Lapierre, Frédéric Cuisinier, Vincent Cavallès, et al.. Adsorption of proteins on TiO₂ particles influences their aggregation and cell penetration. Food Chemistry, 2021, 360, pp.130003. 10.1016/j.foodchem.2021.130003 . hal-03358586

HAL Id: hal-03358586

<https://hal.science/hal-03358586>

Submitted on 29 Sep 2021

HAL is a multi-disciplinary open access archive for the deposit and dissemination of scientific research documents, whether they are published or not. The documents may come from teaching and research institutions in France or abroad, or from public or private research centers.

L'archive ouverte pluridisciplinaire **HAL**, est destinée au dépôt et à la diffusion de documents scientifiques de niveau recherche, publiés ou non, émanant des établissements d'enseignement et de recherche français ou étrangers, des laboratoires publics ou privés.

25 **1. Introduction**

26 Nanoparticles (NP) are commonly used in food as texturing and flavor agents (McCracken et al.,
27 2016). One widely used additive is the food grade TiO₂ also identified as E171, which is found in
28 various food products (including candies and chocolate bars) as well as toothpaste. In 2012, a
29 simulation of TiO₂ consumption emphasizes that children below 10 years old are the most exposed
30 individuals (Weir et al., 2012). TiO₂ is also used for packaging and, in that case, food can be
31 contaminated by the packing (Lin et al., 2014). The question about the innocuousness of TiO₂
32 nanoparticles (TiO₂ NP) is not new since in 2011, Skocaj et al. addressed the question: "Titanium
33 dioxide in our everyday life; is it safe?" (Skocaj et al., 2011). Closer than 10 years after, the impact
34 of food grade TiO₂ on health is not totally elucidated and there is a need for interdisciplinary
35 approaches to understand organ/NP interaction (Chaudhry et al., 2008).

36 Numerous effects of TiO₂ have been reported on different organs such as liver, brain, intestines
37 or spleen (Jovanović, 2015). The TiO₂ NPs are known as inducers of inflammation in several organs
38 such as kidney (Gui et al., 2011). In addition, genotoxicity has been observed for numerous
39 structures of TiO₂ NPs (including anatase and rutile) with different exposure modes (ingestion,
40 inhalation...) (Shi et al., 2013). The TiO₂ NPs induce oxidative damages to DNA. The E171 toxicity
41 on intestinal cells is moderated but sufficient to suggest a role in tumor growth in the colon of
42 mice (Dorier et al., 2017; Proquin et al., 2018). Moreover, E171 is suspected to worsen existing
43 intestinal disease (Urrutia-Ortega et al., 2016). Indeed, the sedimentation of TiO₂ could induce a
44 loss of intestinal microvilli (Faust et al., 2014) and a slight deregulation of the fatty acids profiles
45 in the intestine. However, the TiO₂ NPs do not seem to impact the bacteria gas production
46 (Dudefoi et al., 2017). Finally, in cells, TiO₂ NPs were found to disrupt the structure of lysosomes
47 and to damage the mitochondria (Zhang et al., 2018) and could have synergy action with food
48 molecules such as glucose (Wang et al., 2013).

49 The relevant properties which explain NP toxicity are their solubility, shape, surface charge, size
50 distribution and structure (McCracken et al., 2016). Cell penetration was reported after dermal
51 exposure and in hairless skin, TiO₂ NPs were found in epidermis cells (Wu et al., 2009). Basically,
52 TiO₂ NPs can penetrate in cells as shown for MCF-7 and TERT cells using confocal Raman
53 spectroscopy (Salehi et al., 2014). Recently, debate around the use of TiO₂ in food was revived. In
54 2017, Bettini et al. reported that after 100 days, the TiO₂ nanoparticles initiate preneoplastic
55 lesions and promote colon inflammation. This suggested a potential role of TiO₂ NPs in
56 autoimmune disease and colorectal cancers (Bettini et al., 2017). Following this publication, the
57 French Agency for Food, Environmental and Occupational Health and Safety has recommended
58 the limitation the TiO₂ as food additive as emergency measure regarding the lack of knowledge
59 about the real toxicity (Anses, 2019).

60 As the other nanoparticles, TiO₂ tends to aggregate in solution. This is enhanced by the presence
61 of salt in the media (Allouni et al., 2009). The ability of proteins to prevent nanoparticle
62 aggregation is well known (Lepoitevin et al., 2015). For noble metals, such property is modulated
63 to design colorimetric sensors (Sabela et al., 2017). The coating of TiO₂ NPs by human serum
64 albumin, bovine serum albumin or fetal bovine serum prevents the aggregation process (Allouni
65 et al., 2009; Yusoff et al., 2018). In their review, McCracken et al. hypothesized that NP coating by
66 protein could be an important factor of their toxicity (McCracken et al., 2016).

67 Protein adsorption on material is a complex and fascinating phenomena whose mechanism is not
68 fully understood after several decades of investigation. However, the structural classification of
69 proteins could be a way to predict their behavior on a flat surface (Coglitore et al., 2019).
70 Numerous parameters affect protein adsorption on nanoparticles such as pH, concentration,
71 temperature, salt concentration (Bhakta et al., 2015) and additional molecules such as polyphenol
72 (Coglitore et al., 2018). Hard proteins such as lysozyme keep their structure after adsorption on

73 solid interface (Balme et al., 2013). Although considered as soft protein, BSA does not unfold on
74 food grade E171 (Kim & Doudrick, 2019). The adsorption of blood proteins on anatase TiO₂ NPs
75 affects the agglomerate size and surface charge. Additionally, this altered the electrostatic binding
76 affinity with fibroblasts (Allouni et al., 2015). Because proteins can strongly interact with TiO₂ NPs,
77 we addressed the question about the consequences of such interaction. Typically, under salted
78 media, NP aggregation reduces the ability of the NP to penetrate inside the cell. Food proteins,
79 by preventing this aggregation process, could therefore enhance the penetration of TiO₂ NPs in
80 the cell. In order to verify this hypothesis, we selected two proteins *i.e.* β-lactoglobulin and gelatin.
81 β-lactoglobulin is mainly composed of β-sheets which provide a high internal energy. In presence
82 of silica or hydrophobic surface, the conformational changes of β-lactoglobulin are small
83 (Wahlgren & Arnebrant, 1990). When β-lactoglobulin is adsorbed on clay, only weak structural
84 modification occur (Assifaoui et al., 2014). The second protein is gelatin, which is widely used in
85 candies mixed with E171. Gelatin interacts with TiO₂ NPs and such interaction has been used to
86 pattern TiO₂ porous microspheres (Liu et al., 2015). However, the main application of gelatin TiO₂
87 composite is food packaging (He et al., 2016).

88 Mostly, intracellular imaging methods, such as electron microscopy, cryoelectron microscopy, and
89 immunofluorescence microscopy, due to the fixation, freezing and use of dyes or biomarkers are
90 destructive and harmful to the cells. As Raman spectroscopy does not need chemical fixation,
91 markers, or genetic modifications, it is considered as a non-invasive imaging method (Klein et al.,
92 2012; Salehi et al., 2013). Raman spectroscopy is based on inelastic scattering of photons from
93 the incident wavelength. The monochromatic light interacting with the sample, produces a
94 Raman spectrum, composing different bands related to the vibrational frequencies of different
95 functional groups. Subsequently every molecule has an exclusive fingerprint or Raman spectrum.
96 The high spatial resolution and possibility of imaging in aqueous environment make Raman

97 microscopy an ideal tool for life and fixed imaging of a single cell (Salehi et al., 2014). The adequate
98 data analysis according to the vibrational spectra of different cellular organelles, anticancer drugs
99 or nanoparticles provides alternative to existing methods for cell imaging under normal
100 physiological conditions (Gulka et al., 2020; Salehi et al., 2018). The unique spectral signature of
101 nanoparticles enable tracing coated/ non-coated TiO₂ cellular penetration.

102 As previously mentioned, the toxicity of TiO₂ was demonstrated on different type cells in vitro as
103 well as in-vivo. In these cases, numerous external parameters can influence the cell penetration
104 of the nanoparticle including the protein adsorption. This work aims to verify for the first time the
105 hypothesis of the role the protein coating on the TiO₂ nanoparticle cell penetration. Indeed, this
106 question is motivated to elucidate the first step mechanism of the tiO₂ toxicity. To do so, gelatin
107 and β-lactoglobulin adsorption on TiO₂ rutile was first investigated to determine their surface
108 concentration and eventual structural modifications. Then, we evaluated the impact of each of
109 the two proteins on TiO₂ NPs aggregation. Finally, the penetration of NPs coated or not with
110 proteins was investigated by confocal Raman microscopy.

111

112 **2. Materials and methods**

113 **a. Preparation of NPs**

114 The titanium dioxide (TiO₂) powder (99% rutile) (SIGMA) was suspended in distilled water at a
115 concentration of 1 mg/ml. The solution was then sonicated for 1 hour at 60°C (ref sonicator: ELMA
116 Ultrasonic Cleaner S100H) to break up any interactions that may have formed between the
117 different particles. Gelatin (L3908) and β-lactoglobulin (G6144) from Sigma were dissolved in
118 distilled water at a concentration of 1 mg/ml and sonicated. Three solutions were prepared at a
119 final concentration of 0.75 mg/ml of TiO₂ NPs: NPs alone, NPs with gelatin and NPs with β-
120 lactoglobulin. In these solutions, the ratio was about 3 TiO₂ NPs to 1 protein. In order to promote

121 the adsorption of these proteins on NPs as effectively as possible, the solutions were placed on
122 an agitator for one hour at room temperature and then stored at 4°C. A sonication of 5 minutes
123 at room temperature for coated rated NPs and one hour at 60°C for unrated uncoated NPs was
124 applied before each use.

125 **b. Characterization of protein adsorption**

126 The interfacial concentration of protein on TiO₂ NPs was obtained by the method of supernatant
127 depletion previously reported (Lepoitevin et al., 2014). Briefly, after incubation, the mixtures
128 containing TiO₂ NPs and proteins were centrifuged (15 min at 15000 rpm). Protein concentration
129 in the supernatant was determined by UV-Vis absorption (Jasco) at 290 nm. The structural
130 modifications of adsorbed protein were characterized by ATR-FTIR (Nexus) under D₂O. The
131 measurement of NP size was performed by Dynamic Light Scattering (DLS) (Nanophox) using a
132 laser light of 632 nm. For each condition or type of NPs, the measurement was carried out in
133 triplicate. Several parameters such as medium (water, DMEM/F12 medium and RPMI medium)
134 condition and time (from day 0 to day 5) were modified between different measurements. The
135 data analysis was done using QuickFit software.

136 **c. Cell culture**

137 HT29 human colon adenocarcinoma cells were grown in DMEM/F12 medium (M1) or RPMI
138 medium (M2) supplemented with 10% FCS, 100U/ml penicillin, 100 mg/ml streptomycin and
139 100 mg/ml sodium pyruvate. For Raman experiments, 3x10⁵ HT-29 cells were cultivated for 24 h
140 onto polished and disinfected calcium fluoride CaF₂ (Crystran Ltd, Dorset, UK) substrates in 35 mm
141 Petri dishes. After cell adherence to the substrate, the cells were incubated with dissolved
142 nanoparticle solutions at 2 µg/mL concentration for one hour. The cells on the CaF₂ substrates
143 were then fixed with 2% PFA (paraformaldehyde) after thorough rinsing with PBS. Cells were kept
144 in PBS and transferred directly for Raman measurements. Before carrying out measurements of

145 TiO₂ on the cells, several reference spectra of the different NP solutions were carried out for 4
146 conditions, TiO₂ powder and the three solutions of TiO₂ coated or not by proteins (NP/NPG/NPL).

147 **d. Analysis of cell penetration by Raman microscopy**

148 ***Raman data acquisition***

149 To collect the Raman spectra, Witec Confocal Raman Microscope System alpha 300R (Witec Inc.,
150 Ulm, Germany) was used. The excitation light in confocal Raman microscopy was generated via a
151 frequency-doubled Nd:YAG lasers (New-port, Irvine, CA, USA) at a wavelength of 532 nm. A 60×
152 NIKON water immersion objective with a numerical aperture of 1.0 and a working distance of
153 2.8 mm (Nikon, Tokyo, Japan) was used to focus the laser beam onto the cells. The laser power
154 after the objective was 15 mW but finally, lower power was absorbed by cells in PBS. The
155 scattered radiation goes through an edge filter to the electron multiplying charge coupled device
156 camera EMCCD (DU 970N-BV353, Andor, Hartford, USA). The EMCCD chip size was 1600 × 200
157 pixels, the camera controller of a 16-bit A/D converter operated at 2.5 MHz. The acquisition time
158 of a single spectrum was set to 0.5 sec. A zone of 150 × 150 pixels (spatial unit) per image was
159 recorded, giving 22500 spectra for one image. Data acquisition and analysis was performed using
160 Image Plus 2.08 Witec software. A spatial resolution of 300 nm and a depth resolution of 1µm
161 were measured for the system. Considering the limit of Raman microscope (300 nm), the
162 measurements of particle sizes on each image (processed and analyzed using Witec software)
163 were done by zooming on particles and using line size measurement tool.

164 ***Raman data analysis***

165 Two data analysis methods have been applied. The first method presented integrated Raman
166 intensities in specific regions in particular C-H stretching mode. The lipid-protein distribution in
167 the cells is shown by the integrated Raman intensities of C-H stretching mode (2800–3000cm⁻¹)
168 using Image Plus software, Witec. Consequently, a map of the region regarding these integrated

169 intensities was provided. A false color image of CH Raman peak contains bright yellow hues for
170 the highest intensities and dark orange hues for the lowest integrated intensities. K-mean cluster
171 analysis (KMCA) as the second data analysis method separated data into k-mutually clusters.
172 KMCA was done using the Witec Project Plus (Ulm, Germany) software.

173 **e. Statistical analysis**

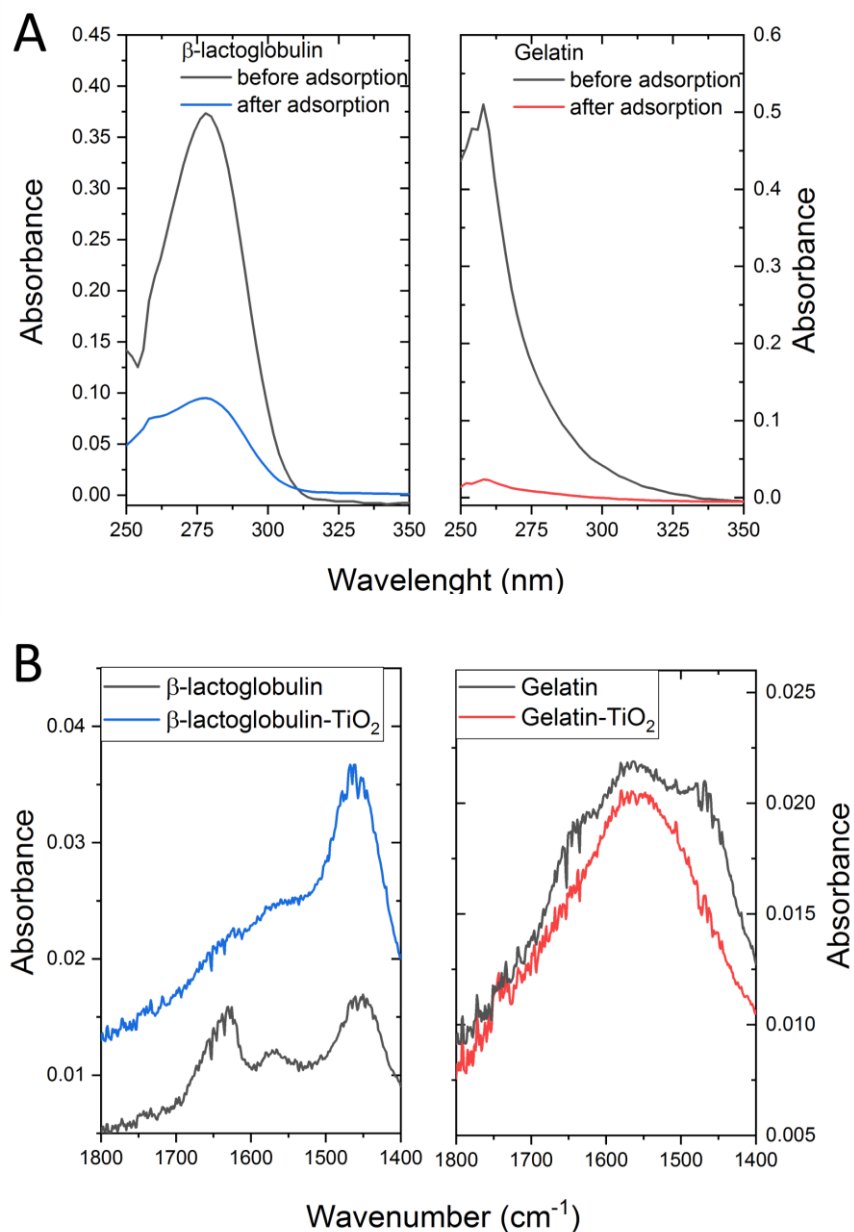
174 All experiments were conducted independently at least three times. Results were expressed as
175 the mean \pm standard error of the mean (S.E.M). Statistical comparisons were performed with one-
176 way ANOVA or t-test as indicated. A probability level (p value) of 0.05 was chosen for statistical
177 significance.

178

179 **3. Results and discussion**

180 **a. Protein adsorption on TiO₂ NPs**

181 Prior to the investigation of the protein impact on colloidal stability and cell penetration, we
182 characterized protein loading on TiO₂ NPs. Indeed, the protein/NP interaction is extremely
183 dependent on the intrinsic properties of the material and on the media. Here, we have used water
184 in order to prevent salt induced aggregation of TiO₂ NPs and thus to optimize the accessible
185 surface of NPs for protein adsorption.



186

187 **Figure 1: (A) Absorbance spectra of β -lactoglobulin (left) and gelatin (right) before (black line)**

188 **and after (red line) contact with TiO_2 NPs at a concentration of 0.75 mg/ml for 1 hour. (B) FTIR**

189 **spectra of β -lactoglobulin (left) and gelatin (right) in D_2O (black line) and loaded on TiO_2 NPs**

190 **(blue or red line)**

191 The interfacial concentration of protein was determined from the depletion of supernatant

192 method. Figure 1A shows the absorbance spectra for β -lactoglobulin and gelatin before and after

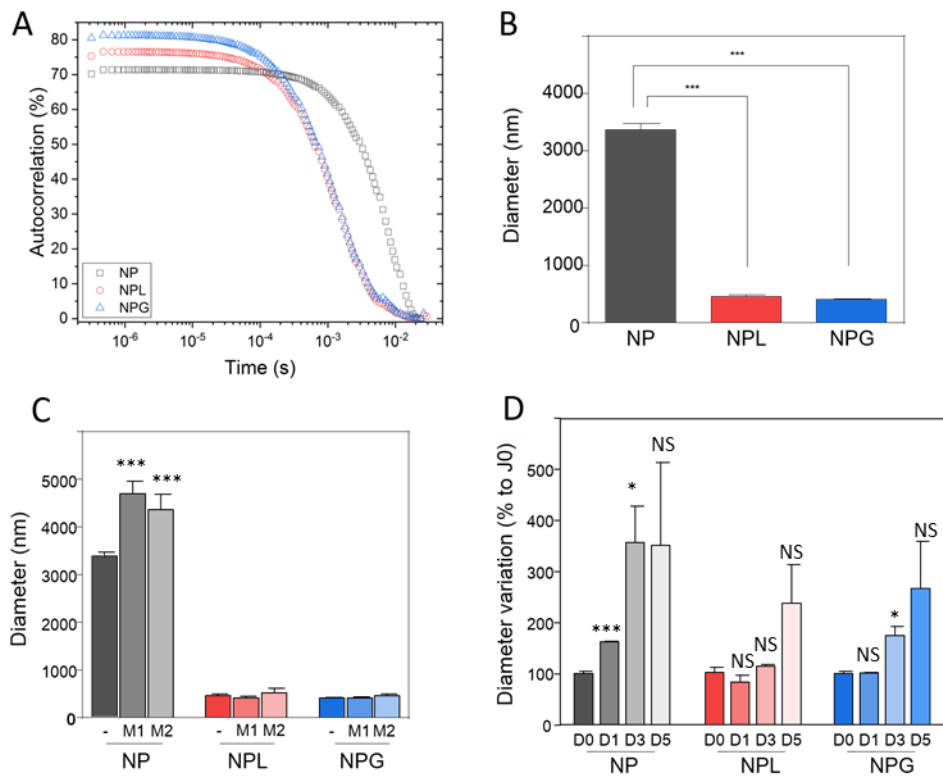
193 adsorption on TiO₂ NPs. We can observe a large decrease of protein concentration in solution
194 upon adsorption. The interfacial concentrations for β-lactoglobulin and gelatin were found about
195 0.25 mg/mg and 0.32 mg/mg of TiO₂ NPs, respectively.

196 We attempted to obtain information about the structural modifications of proteins induced by
197 their adsorption on TiO₂ NPs. In Figure 1B are plotted the FTIR spectra recorded under D₂O. For
198 the β-lactoglobulin, the band in 1640 cm⁻¹ was assigned to the amide I. In D₂O, the amides II gave
199 two bands in 1560 cm⁻¹ and 1455 cm⁻¹ relative to N-H and N-D bonds, respectively. This
200 emphasizes the accessibility to the solvent of the amide II moieties to exchange H by D. After
201 loading on TiO₂ NPs, the 3 bands were still present. Unfortunately, the absorption of Ti-OD bond
202 about 1590 made a deep structural analysis impossible. However, we observed an increase of the
203 band in 1455 cm⁻¹ that could be assigned to the conversion of N-H to N-D. This suggested that the
204 amides I bound with H were more exposed to the solvent after loading on TiO₂ NPs due to
205 structural modifications.

206 For gelatin in D₂O, the 3 bands were also present but more difficult to distinguish because of the
207 low order degree of the protein. However, we noticed that the two bands of amides I were large
208 showing the existence of N-H and N-D bonds. After loading, the band about 1690 cm⁻¹ masked
209 the other ones. Conversely to β-lactoglobulin, the adsorption of gelatin did not seem to promote
210 the exposition of the amides II to the solution.

211 **b. Colloidal stability of TiO₂ NPs with and without protein loading**

212 As previously mentioned, the colloidal stability of TiO₂ NPs could strongly be affected by protein
213 adsorption. Importantly, this is also a key factor for cell penetration. Thus, we then investigated
214 by dynamic light scattering the TiO₂ NP size, in water and in two cell culture media.



215

216 **Figure 2: Nanoparticle size by diffusion light scattering (A) Autocorrelation function of TiO₂ NPs**
 217 **without (black) and with protein (in red, β-lactoglobulin and in blue, gelatin). The sizes of TiO₂**
 218 **NPs are obtained in water (B) and culture media (DMEM/F12 medium (M1) or RPMI medium**
 219 **(M2)) (C). (D) Size evolution of the small component as a function of time (From Day 0 to Day**
 220 **5). TiO₂ NPs alone is noted NP, TiO₂ NPs with gelatin is noted NPG and TiO₂-NPs with β-**
 221 **lactoglobulin is noted NPL. Statistical significance is shown as p-value from one-way Anova test**
 222 **(panels B and C) or t-test in panel D (*: p<0.05; ***: p<0.001).**

223

224 In Figure 2A, the autocorrelation functions for TiO₂ NPs in water, with and without proteins are
 225 reported. We observed a shift toward short times when TiO₂ NPs were coated with proteins. At
 226 first approximation, the autocorrelation functions were fitted with only one component to obtain
 227 an average size distribution. For uncoated TiO₂ NPs, the distribution was centered around 3.2 μm

228 while after protein coating it was about 400 nm (Figure 2B). This is due to a rapid aggregation of
229 TiO₂ NPs after sonication. Here, we can note that both gelatin and β-lactoglobulin prevented the
230 fast aggregation phenomena of TiO₂ NPs.

231 In general, NP aggregation is favored by salt addition. Thus, similar analyses were performed using
232 two different media used for cell culture (Figure 2C). This experiment was also motivated because
233 the role of protein loading cannot be predicted since it is dependent on the protein and the
234 eventual binding with small molecules, as shown for gold NP (Coglitore et al., 2018; Lepoitevin et
235 al., 2015) or clay mineral (Trigueiro et al., 2018).

236 As expected, the size of raw TiO₂ NPs increased due to salt-induced aggregation. Conversely,
237 coating with proteins appeared to prevent the aggregation process. These results agree with
238 previous investigations showing that the extracellular polymeric substances from *Bacillus subtilis*
239 improve the colloidal stability of TiO₂ NPs (Di Lin et al., 2017; Di Lin et al., 2016). Gelatin has a low
240 internal energy structure and thus can optimize its conformation around the TiO₂ NPs. Conversely,
241 β-lactoglobulin is mainly composed of β-sheet, has a high internal energy and is positively charged
242 at pH 7.4. However, the FTIR revealed structural modifications, which probably allowed the
243 interaction between the protein and TiO₂ NPs. This means that the electrostatic interaction
244 between the TiO₂ NPs and β-lactoglobulin are not shielded by salt addition thus explaining the
245 colloidal stability.

246 TiO₂ NPs penetrate inside cells only if their size are hundreds nanometer scale. The low accuracy
247 of the autocorrelation fit with only one component suggested a polydispersity of the samples. To
248 further analysis the size of TiO₂ NPs, we separated two populations from the autocorrelation
249 curves. A first population with a diameter below 100 nm was assigned to non-aggregated
250 particles. The second population micrometer scale corresponded to aggregates. The relative
251 weight of each population showed that non-aggregated particles were the main one (upper than

252 99%), for the TiO₂ NPs coated with proteins. We then focused on this population more prone to
253 penetrate inside the cells. The stability of these small TiO₂ NPs as a function of time was
254 investigated for duration up to 5 days (Figure 2D). Without protein coating, TiO₂ NPs were prone
255 to aggregate with time as monitored by the diameter variation as a function of the time. Typically,
256 at D0 the mean size of the TiO₂-NP was about 100 nm and reached 480 nm after D5. This is not
257 surprising since TiO₂ NPs are not stable in solution. With gelatin, the TiO₂ NPs size was stable until
258 D1 around 91 nm. Then, the diameter variation increased to reach 250 % at D5. Finally, β-
259 lactoglobulin offered the most effective protection against aggregation since the size of NPL
260 particles remained constant during the 3-days.

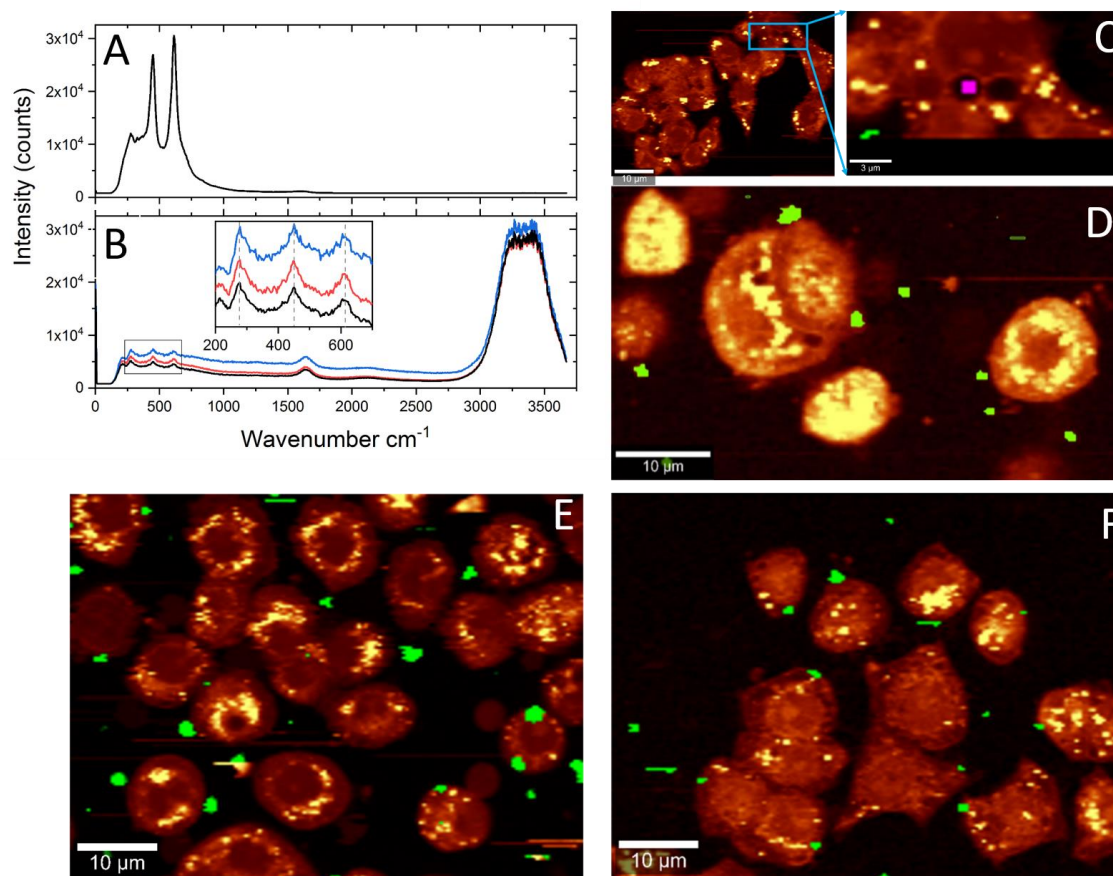
261 At this stage, we demonstrated that protein coating prevented the TiO₂ NPs aggregation in water
262 as well as in salt media. On the other hand, the colloidal stability was also improved during the
263 time especially for the β-lactoglobulin.

264 **c. Effect of proteins on cell penetration of TiO₂ NPs**

265 To find out the role of protein, intracellular penetration of TiO₂ NPs was investigated using the
266 human intestinal epithelial cell lines HT-29, cultured in DMEM-F12 medium. The characterization
267 of TiO₂ NPs and their location were obtained using confocal Raman microscopy.

268 The Raman spectrum of TiO₂ powder showed three significant peaks at 275 cm⁻¹, 450 cm⁻¹ and
269 610 cm⁻¹ (Figure 3A). Coated/non-coated TiO₂ NPs in solution, showed the same peak position
270 confirming the integrity of TiO₂ NPs. The low intensities of TiO₂ NPs coated with proteins (blue and
271 red line for NPG and NPL, respectively) peaks were due to the coating, which avoids particles
272 accumulation and lower Raman signal. In addition, powder signal was higher as compared to the
273 NP in solution, as the number of particles under the laser spot was lower for the floating particles
274 in solution.

275



276

277 **Figure 3: Raman spectra of (A) TiO₂ powder, (B) TiO₂-NPs (black line), TiO₂-NPs with gelatin (blue**
 278 **line) and TiO₂-NPs with β-lactoglobulin (red line), the inset is a zoom of 200 cm⁻¹ – 700 cm⁻¹**
 279 **region. (C) Integration over Raman intensities of CH region, HT-29 cells incubated with TiO₂**
 280 **NPGs and selected areas to focus on the TiO₂ presence inside the cell in pink color and outside**
 281 **in green. The image (D), (E) and (F) were obtained in presence of TiO₂-NPs, TiO₂-NPs with gelatin**
 282 **and TiO₂-NPs with β-lactoglobulin respectively.**

283

284 Figure 3(B-E) illustrates the image acquisition of cells in presence of TiO₂ NPs with and without
 285 protein coating. Raman images present the biomolecules and two clusters in pink (intracellular
 286 penetrated particles) and green (extracellular particles). The intensity of CH bonds is plotted in
 287 yellow hues have the maximum intensity (for proteins or lipids) and dark hues have zero intensity

288 of CH bonds (background and out of cells). After 1 hour incubation of HT-29 cells with raw
289 nanoparticles, TiO₂ NPs aggregates were mainly present outside the cell or were in interaction
290 with the cell membrane. Conversely, TiO₂ NPs coated with proteins were found inside the cells
291 suggesting that protein coating favored cell penetration. We also noticed that TiO₂ NPs coated
292 with proteins were more abundant as compared to the particles without coating.

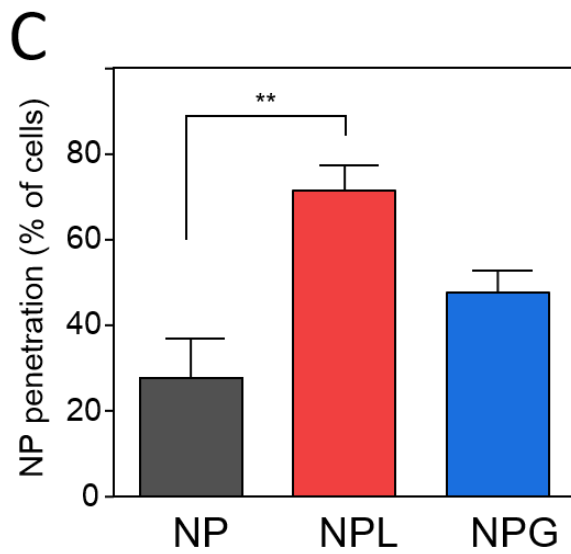
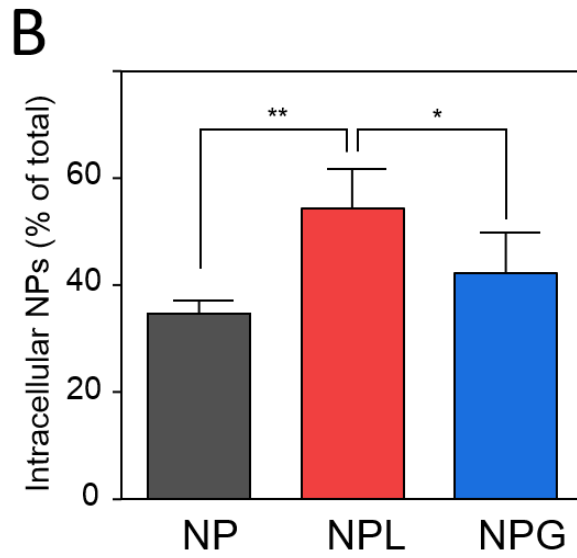
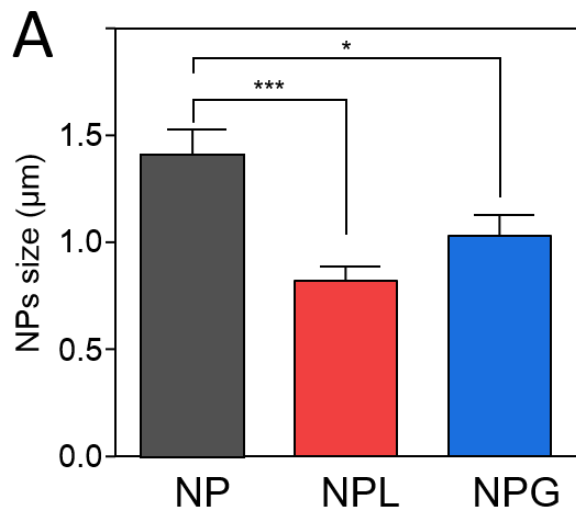
293 Further analysis reported on Figure 4 shows the percentage of total penetration of
294 coated/noncoated NPs. The quantification was obtained from a total number of 296 cells from all
295 the Raman images that were analyzed. The average size of TiO₂ NPs inside the cells showed that
296 the raw TiO₂ NPs were larger (1.4 μm) than the coated TiO₂ NPs (1 μm and 0.8 μm for gelatin and
297 β-lactoglobulin, respectively). The spatial resolution of Raman microscopy is 300 nm and thus a
298 discrepancy between the DLS is not surprising. Indeed, the Raman microscopy provides
299 information on several nanoparticles that can count one by one as soon as their size is larger than
300 the resolution while the DLS provides a means measurement of the nanoparticle size that can be
301 distorted in the case of heterogeneous samples. However, the tendency between confocal Raman
302 microscopy results and DLS measurements were in good agreement.

303 We also quantified the percentage of NPs that penetrated inside the cells (Figure 4B and C). For
304 the raw TiO₂ NPs, 35% of particles were located inside HT-29 cells. This ratio increased up to 42%
305 and 55% when the TiO₂ NPs were coated with gelatin or β-lactoglobulin, respectively. Such
306 enhancement of cell penetration induced by protein coating was significant and probably linked,
307 at least in part, to the difference in size of the three types of NPs. We also evaluated the
308 distribution of TiO₂ NPs in the cell population. Without proteins, the TiO₂ NPs penetrated only 28%
309 of the cells. The coating with protein favored the dissemination of TiO₂ NPs since 48% and 70% of
310 cells showed internalized TiO₂ NPs after coating with gelatin and β-lactoglobulin, respectively. The

311 difference between the two proteins can be assigned to their ability to prevent the TiO₂ NPs
312 aggregation.

313 As demonstrated, confocal Raman microscopy with high spatial resolution allowed us to analyze
314 and trace coated/non-coated TiO₂ nanoparticles. This label-free method using the spectral
315 fingerprint of nanoparticles permitted the monitoring of their intracellular penetration. The
316 results obviously present the significant difference between coated particles agglomeration and
317 penetration. Non-coated TiO₂ are more prone to aggregation and therefore their intracellular
318 penetration was lower. Conversely, protein adsorption prevented the TiO₂ NPs aggregation and
319 thus favored cell penetration.

320



322 **Figure 4: Characterization of TiO₂ NP penetration inside HT-29 cells (A) NP size, (B) ratio of**
323 **intracellular TiO₂ NPs and (C) percentage of cells containing TiO₂ NPs. TiO₂ NPs alone is noted**
324 **NP, TiO₂ NPs with gelatin is noted NPG, and TiO₂ NPs with β -lactoglobulin is noted NPL.**
325 **Statistical significance is shown as p-value from one-way Anova test (*: $p < 0.05$; **: $p <$**
326 **0.01;***: $p < 0.001$).**

327

328 **4. Conclusion**

329 To sum up, we investigated the impact of protein adsorption on cell penetration of TiO₂ NPs. Our
330 results showed that both β -lactoglobulin and gelatin were loaded on TiO₂ NPs. The FTIR suggested
331 that β -lactoglobulin (but not gelatin) adsorption induced a structural modification. The salt-
332 induced aggregation and the colloidal stability were improved by protein adsorption. The cell
333 penetration investigated by confocal Raman microscopy revealed that the β -lactoglobulin favored
334 more efficiently than gelatin TiO₂ NP cell penetration. Moreover, our results showed a correlation
335 between the ability of proteins to prevent NP aggregation and to facilitate cell penetration.

336 Overall, this work proves that proteins present in food have a significant impact on TiO₂ NP
337 penetration in human intestinal epithelial cells. This tends to reinforce the hypothesis that NP
338 coating by proteins could be an important factor explaining their toxicity. Thus, in further
339 investigations aiming to understand the toxicity of TiO₂ NP, the role of food proteins should be
340 taken into account.

341

342 **Acknowledgments**

343 This work was supported by the INCa-Cancéropole GSO (grant 2018-E02). Raman microscopy
344 analysis during this study was realized using the EDMOS platform which was created with the

345 financial support of the Region Occitanie (France) and the European Regional Development Fund
346 (ERDF).

347

348

349

350 **References**

- 351 Allouni, Z. E., Cimpan, M. R., Høl, P. J., Skodvin, T., & Gjerdet, N. R. (2009). Agglomeration and
352 sedimentation of TiO₂ nanoparticles in cell culture medium. *Colloids and surfaces. B,*
353 *Biointerfaces*, *68*, 83–87.
- 354 Allouni, Z. E., Gjerdet, N. R., Cimpan, M. R., & Høl, P. J. (2015). The effect of blood protein
355 adsorption on cellular uptake of anatase TiO₂ nanoparticles. *International journal of*
356 *nanomedicine*, *10*, 687–695.
- 357 Anses (2019). ANSES OPINION on the risks associated with ingestion of the food additive E171.
358 Assifaoui, A., Huault, L., Maissiat, C., Roullier-Gall, C., Jeandet, P., Hirschinger, J., Raya, J., Jaber,
359 M., Lambert, J.-F., Cayot, P., Gougeon, R. D., & Loupiac, C. (2014). Structural studies of
360 adsorbed protein (betalactoglobulin) on natural clay (montmorillonite). *RSC Adv*, *4*, 61096–
361 61103.
- 362 Balme, S., Guégan, R., Janot, J.-M., Jaber, M., Lepoitevin, M., Dejardin, P., Bourrat, X., &
363 Motelica-Heino, M. (2013). Structure, orientation and stability of lysozyme confined in
364 layered materials. *Soft Matter*, *9*, 3188.
- 365 Bettini, S., Boutet-Robinet, E., Cartier, C., Coméra, C., Gaultier, E., Dupuy, J., Naud, N., Taché, S.,
366 Gysan, P., Reguer, S., Thieriet, N., Réfrégiers, M., Thiaudière, D., Cravedi, J.-P., Carrière, M.,
367 Audinot, J.-N., Pierre, F. H., Guzylack-Piriou, L., & Houdeau, E. (2017). Food-grade TiO₂
368 impairs intestinal and systemic immune homeostasis, initiates preneoplastic lesions and
369 promotes aberrant crypt development in the rat colon. *Scientific reports*, *7*, 40373.
- 370 Bhakta, S. A., Evans, E., Benavidez, T. E., & Garcia, C. D. (2015). Protein adsorption onto
371 nanomaterials for the development of biosensors and analytical devices: a review. *Analytica*
372 *chimica acta*, *872*, 7–25.
- 373 Chaudhry, Q., Scotter, M., Blackburn, J., Ross, B., Boxall, A., Castle, L., Aitken, R., & Watkins, R.
374 (2008). Applications and implications of nanotechnologies for the food sector. *Food*
375 *additives & contaminants. Part A, Chemistry, analysis, control, exposure & risk assessment*,
376 *25*, 241–258.
- 377 Coglitore, D., Giambianco, N., Kizalaité, A., Coulon, P. E., Charlot, B., Janot, J.-M., & Balme, S.
378 (2018). Unexpected Hard Protein Behavior of BSA on Gold Nanoparticle Caused by
379 Resveratrol. *Langmuir the ACS journal of surfaces and colloids*, *34*, 8866–8874.
- 380 Coglitore, D., Janot, J.-M., & Balme, S. (2019). Protein at liquid solid interfaces: Toward a new
381 paradigm to change the approach to design hybrid protein/solid-state materials. *Advances in*
382 *colloid and interface science*, *270*, 278–292.
- 383 Di Lin, Drew Story, S., Walker, S. L., Huang, Q., & Cai, P. (2016). Influence of extracellular
384 polymeric substances on the aggregation kinetics of TiO₂ nanoparticles. *Water research*,
385 *104*, 381–388.

386 Di Lin, Story, S. D., Walker, S. L., Huang, Q., Liang, W., & Cai, P. (2017). Role of pH and ionic
387 strength in the aggregation of TiO₂ nanoparticles in the presence of extracellular polymeric
388 substances from *Bacillus subtilis*. *Environmental pollution (Barking, Essex 1987)*, *228*, 35–42.

389 Dorier, M., Béal, D., Marie-Desvergne, C., Dubosson, M., Barreau, F., Houdeau, E., Herlin-Boime,
390 N., & Carriere, M. (2017). Continuous in vitro exposure of intestinal epithelial cells to E171
391 food additive causes oxidative stress, inducing oxidation of DNA bases but no endoplasmic
392 reticulum stress. *Nanotoxicology*, 1–11.

393 Dufefoi, W., Moniz, K., Allen-Vercoe, E., Ropers, M.-H., & Walker, V. K. (2017). Impact of food
394 grade and nano-TiO₂ particles on a human intestinal community. *Food and chemical
395 toxicology an international journal published for the British Industrial Biological Research
396 Association*, *106*, 242–249.

397 Faust, J. J., Doudrick, K., Yang, Y., Westerhoff, P., & Capco, D. G. (2014). Food grade titanium
398 dioxide disrupts intestinal brush border microvilli in vitro independent of sedimentation. *Cell
399 biology and toxicology*, *30*, 169–188.

400 Gui, S., Zhang, Z., Zheng, L., Cui, Y., Liu, X., Li, N., Sang, X., Sun, Q., Gao, G., Cheng, Z., Cheng, J.,
401 Wang, L., Tang, M., & Hong, F. (2011). Molecular mechanism of kidney injury of mice caused
402 by exposure to titanium dioxide nanoparticles. *Journal of hazardous materials*, *195*, 365–
403 370.

404 Gulka, M., Salehi, H., Varga, B., Middendorp, E., Pall, O., Raabova, H., Cloitre, T., Cuisinier, F. J.
405 G., Cigler, P., Nesladek, M., & Gergely, C. (2020). Simultaneous label-free live imaging of cell
406 nucleus and luminescent nanodiamonds. *Scientific reports*, *10*, 9791.

407 He, Q., Zhang, Y., Cai, X., & Wang, S. (2016). Fabrication of gelatin-TiO₂ nanocomposite film and
408 its structural, antibacterial and physical properties. *International journal of biological
409 macromolecules*, *84*, 153–160.

410 Jovanović, B. (2015). Critical review of public health regulations of titanium dioxide, a human
411 food additive. *Integrated environmental assessment and management*, *11*, 10–20.

412 Kim, J., & Doudrick, K. (2019). Emerging investigator series: protein adsorption and
413 transformation on catalytic and food-grade TiO₂ nanoparticles in the presence of dissolved
414 organic carbon. *Environmental Science: Nano*, *6*, 1688–1703.

415 Klein, K., Gigler, A. M., Aschenbrenner, T., Monetti, R., Bunk, W., Jamitzky, F., Morfill, G., Stark,
416 R. W., & Schlegel, J. (2012). Label-free live-cell imaging with confocal Raman microscopy.
417 *Biophysical journal*, *102*, 360–368.

418 Lepoitevin, M., Jaber, M., Guégan, R., Janot, J.-M., Dejardin, P., Henn, F., & Balme, S. (2014). BSA
419 and lysozyme adsorption on homoionic montmorillonite: Influence of the interlayer cation.
420 *Applied Clay Science*, *95*, 396–402.

421 Lepoitevin, M., Lemouel, M., Bechelany, M., Janot, J.-M., & Balme, S. (2015). Gold nanoparticles
422 for the bare-eye based and spectrophotometric detection of proteins, polynucleotides and
423 DNA. *Microchimica Acta*, *182*, 1223–1229.

424 Lin, Q.-B., Li, H., Zhong, H.-N., Zhao, Q., Xiao, D.-H., & Wang, Z.-W. (2014). Migration of Ti from
425 nano-TiO₂-polyethylene composite packaging into food simulants. *Food additives &
426 contaminants. Part A, Chemistry, analysis, control, exposure & risk assessment*, *31*, 1284–
427 1290.

428 Liu, B., Xiao, J., Xu, L., Yao, Y., Costa, B. F.O., Domingos, V. F., Ribeiro, E. S., Shi, F.-N., Zhou, K.,
429 Su, J., Wu, H., Zhong, K., Paixão, J. A., & Gil, J. M. (2015). Gelatin-assisted sol-gel derived
430 TiO₂ microspheres for hydrogen storage. *International Journal of Hydrogen Energy*, *40*,
431 4945–4950.

432 McCracken, C., Dutta, P. K., & Waldman, W. J. (2016). Critical assessment of toxicological effects
433 of ingested nanoparticles. *Environmental Science: Nano*, *3*, 256–282.

434 Proquin, H., Jetten, M. J., Jonkhout, M. C. M., Garduño-Balderas, L. G., Briedé, J. J., Kok, T. M. de,
435 Chirino, Y. I., & van Loveren, H. (2018). Gene expression profiling in colon of mice exposed to
436 food additive titanium dioxide (E171). *Food and chemical toxicology an international journal*
437 *published for the British Industrial Biological Research Association*, *111*, 153–165.

438 Sabela, M., Balme, S., Bechelany, M., Janot, J.-M., & Bisetty, K. (2017). A Review of Gold and
439 Silver Nanoparticle-Based Colorimetric Sensing Assays. *Advanced Engineering Materials*, *19*,
440 1700270.

441 Salehi, H., Al-Arag, S., Middendorp, E., Gergely, C., Cuisinier, F., & Orti, V. (2018). Dental pulp
442 stem cells used to deliver the anticancer drug paclitaxel. *Stem cell research & therapy*, *9*,
443 103.

444 Salehi, H., Calas-Bennasar, I., Durand, J.-C., Middendorp, E., Valcarcel, J., Larroque, C., Nagy, K.,
445 Turzó K, K., Dekany, I., & Cuisinier, F. J. G. (2014). Confocal Raman spectroscopy to monitor
446 intracellular penetration of TiO₂ nanoparticles. *Journal of Raman Spectroscopy*, *45*, 807–
447 813.

448 Salehi, H., Derely, L., Vegh, A.-G., Durand, J.-C., Gergely, C., Larroque, C., Fauroux, M.-A., &
449 Cuisinier, F. J. G. (2013). Label-free detection of anticancer drug paclitaxel in living cells by
450 confocal Raman microscopy. *Applied Physics Letters*, *102*, 113701.

451 Shi, H., Magaye, R., Castranova, V., & Zhao, J. (2013). Titanium dioxide nanoparticles: a review of
452 current toxicological data. *Particle and fibre toxicology*, *10*, 15.

453 Skocaj, M., Filipic, M., Petkovic, J., & Novak, S. (2011). Titanium dioxide in our everyday life; is it
454 safe? *Radiology and oncology*, *45*, 227–247.

455 Trigueiro, P., Pedetti, S., Rigaud, B., Balme, S., Janot, J.-M., Dos Santos, I. M. G., Gougeon, R.,
456 Fonseca, M. G., Georgelin, T., & Jaber, M. (2018). Going through the wine fining: Intimate
457 dialogue between organics and clays. *Colloids and surfaces. B, Biointerfaces*, *166*, 79–88.

458 Urrutia-Ortega, I. M., Garduño-Balderas, L. G., Delgado-Buenrostro, N. L., Freyre-Fonseca, V.,
459 Flores-Flores, J. O., González-Robles, A., Pedraza-Chaverri, J., Hernández-Pando, R.,
460 Rodríguez-Sosa, M., León-Cabrera, S., Terrazas, L. I., van Loveren, H., & Chirino, Y. I. (2016).
461 Food-grade titanium dioxide exposure exacerbates tumor formation in colitis associated
462 cancer model. *Food and chemical toxicology an international journal published for the British*
463 *Industrial Biological Research Association*, *93*, 20–31.

464 Wahlgren, M., & Arnebrant, T. (1990). Adsorption of β -Lactoglobulin onto silica, methylated
465 silica, and polysulfone. *Journal of Colloid and Interface Science*, *136*, 259–265.

466 Wang, Y., Chen, Z., Ba, T., Pu, J., Chen, T., Song, Y., Gu, Y., Qian, Q., Xu, Y., Xiang, K., Wang, H., &
467 Jia, G. (2013). Susceptibility of young and adult rats to the oral toxicity of titanium dioxide
468 nanoparticles. *Small (Weinheim an der Bergstrasse, Germany)*, *9*, 1742–1752.

469 Weir, A., Westerhoff, P., Fabricius, L., Hristovski, K., & Goetz, N. von (2012). Titanium dioxide
470 nanoparticles in food and personal care products. *Environmental science & technology*, *46*,
471 2242–2250.

472 Wu, J., Liu, W., Xue, C., Zhou, S., Lan, F., Bi, L., Xu, H., Yang, X., & Zeng, F.-D. (2009). Toxicity and
473 penetration of TiO₂ nanoparticles in hairless mice and porcine skin after subchronic dermal
474 exposure. *Toxicology letters*, *191*, 1–8.

475 Yusoff, R., Kathawala, M. H., Nguyen, L. T.H., Setyawati, M. I., Chiew, P., Wu, Y., Ch'ng, A. L.,
476 Wang, Z. M., & Ng, K. W. (2018). Biomolecular interaction and kinematics differences
477 between P25 and E171 TiO₂ nanoparticles. *NanoImpact*, *12*, 51–57.

478 Zhang, Y., Xu, B., Yao, M., Dong, T., Mao, Z., Hang, B., Han, X., Lin, Z., Bian, Q., Li, M., & Xia, Y.
479 (2018). Titanium dioxide nanoparticles induce proteostasis disruption and autophagy in
480 human trophoblast cells. *Chemico-biological interactions*, *296*, 124–133.

481